Journal of Biomechanics 82 (2019) 375–380

Contents lists available at ScienceDirect

Journal of Biomechanics

journal homepage: www.elsevier.com/locate/jbiomech
www.JBiomech.com

Short communication

# MRI vs CT-based 2D-3D auto-registration accuracy for quantifying shoulder motion using biplane video-radiography

Mohsen Akbari-Shandiz [a,b], Rebekah L. Lawrence [b], Arin M. Ellingson [b], Casey P. Johnson [c], Kristin D. Zhao [a], Paula M. Ludewig [b,*]

[a] Assistive and Restorative Technology Laboratory, Rehabilitation Medicine Research Center, Department of Physical Medicine & Rehabilitation, Mayo Clinic, Rochester, MN, USA
[b] Department of Rehabilitation Medicine, Divisions of Rehabilitation Science and Physical Therapy, Medical School, University of Minnesota, MN, USA
[c] Center for Magnetic Resonance Research, University of Minnesota, Minneapolis, MN, USA

ARTICLE INFO

*Article history:*
Accepted 24 September 2018

*Keywords:*
Glenohumeral kinematics
Automatic 2D-3D registration
Shoulder motion tracking
Motion tracking accuracy
Radiostereometric analysis (RSA)

ABSTRACT

Biplane 2D-3D registration approaches have been used for measuring 3D, *in vivo* glenohumeral (GH) joint kinematics. Computed tomography (CT) has become the gold standard for reconstructing 3D bone models, as it provides high geometric accuracy and similar tissue contrast to video-radiography. Alternatively, magnetic resonance imaging (MRI) would not expose subjects to radiation and provides the ability to add cartilage and other soft tissues to the models. However, the accuracy of MRI-based 2D-3D registration for quantifying glenohumeral kinematics is unknown. We developed an automatic 2D-3D registration program that works with both CT- and MRI-based image volumes for quantifying joint motions. The purpose of this study was to use the proposed 2D-3D auto-registration algorithm to describe the humerus and scapula tracking accuracy of CT- and MRI-based registration relative to radiostereometric analysis (RSA) during dynamic biplanar video-radiography. The GH kinematic accuracy (RMS error) was 0.6–1.0 mm and 0.6–2.2° for the CT-based registration and 1.4–2.2 mm and 1.2–2.6° for MRI-based registration. Higher kinematic accuracy of CT-based registration was expected as MRI provides lower spatial resolution and bone contrast as compared to CT and suffers from spatial distortions. However, the MRI-based registration is within an acceptable accuracy for many clinical research questions.


## 1. Introduction

Measuring three-dimensional (3D) *in vivo* glenohumeral joint kinematics accurately is important because it allows for quantification of small changes in clinically relevant parameters such as joint positions/translations, subacromial space, or contact paths of the humerus on the surface of the glenoid. Radiostereometric analysis (RSA) or bone-fixed sensors are considered the gold standard for measuring *in vivo* 3D joint kinematics; however, they are invasive because they require surgically implanting metallic beads or pins into bones (Ludewig et al., 2009; Tashman et al., 2004). Alternatively, 2D-3D registration using biplane video-radiography does not require invasive procedures and is able to provide submillimeter kinematic accuracy (Akbari-Shandiz et al., 2018; Anderst et al., 2008; Bey et al., 2006; Giphart et al., 2012; Massimini et al., 2011; Zhu et al., 2012). In this approach, computed tomography (CT) has become the gold standard for reconstruction of 3D bone models. However, many research situations exist in which kinematic analysis requires repeated imaging of subjects before and after an intervention. Non-diagnostic CT scanning of human volunteers is not always ethically justifiable and permitted as it exposes the subjects to non-therapeutic radiation (Semelka et al., 2007).

Magnetic resonance imaging (MRI) is one possible alternative which does not expose subjects to radiation and provides the ability to add cartilage and other soft tissues to the models. However, MRI provides lower bone contrast compared to CT and suffers from spatial distortions potentially impacting the utility of the model for 2D-3D registration. Auto-registering MRI image volumes to video-radiography images is also very challenging because MRI has fundamental differences in imaging physics compared to the radiography images. The MRI voxel intensity values have no physical meaning, whereas in the radiography and CT images, the intensity value reflects the material density. Therefore, there is not a direct relationship between voxel values of the radiography images and 2D projections of MRI.

* Corresponding author at: Department of Rehabilitation Medicine, Division of Physical Therapy, MMC 388, 420 Delaware St. SE, University of Minnesota, Minneapolis 55455, MN, USA.
*E-mail address:* ludew001@umn.edu (P.M. Ludewig).

https://doi.org/10.1016/j.jbiomech.2018.09.019
0021-9290/

Glenohumeral (GH) kinematic measurement accuracy using CT-based 2D-3D registration has been studied (Bey et al., 2006; Giphart et al., 2012; Massimini et al., 2011; Zhu et al., 2012). However, validation of GH kinematic accuracy using MRI–based registration has never been done, to our knowledge. An automatic 2D-3D registration program was developed that works with both CT- and MRI-based image volumes for quantifying joint motions. The purpose of this study was to describe the humerus and scapula tracking accuracy of CT- and MRI-based registration relative to RSA during dynamic biplanar video-radiography, using 2D-3D auto-registration.

## 2. Methods

### 2.1. Image acquisition

A custom-built biplane video-radiography setup was used for all 2D dynamic imaging (Appendix A) (Imaging Systems and Services Inc.; St. Painesville, OH). A marker grid was used to correct distortion introduced by the image intensifiers. A custom Plexiglas calibration cube was imaged to determine the orientation of the x-ray sources and detectors (Brainerd et al., 2010).

### 2.2. Validation study

With the approval from our institutional biospecimens committee, six cadaveric shoulders (from two male and one female fresh-frozen cadaveric torsos; mean age: 64 years.), were imaged. Shoulder MRI scans were acquired on a 3 T scanner (Siemens Prisma_fit; Siemens Healthcare; Erlangen, Germany) using a shoulder receiver coil array and a T1-weighted VIBE sequence developed to produce 3D models with high geometric accuracy in short acquisition times (Rofsky et al., 1999). Typical scan parameters were: FOV = 210 × 210 × 100 $mm^3$; resolution = 0.82 × 0.82 × 0.89 $mm^3$; TR = 7.16 ms; TE = 2.66 ms; flip angle = 10°; BW = 300 Hz/px; averages = 2; water excitation; elliptical scanning; asymmetric echo; 2D distortion correction; and scan time = 5 min.

Tantalum beads with a diameter of 1.6 mm were implanted into the humerus and scapula of the shoulders. The cadaveric torsos were fixed to a custom apparatus that allowed unconstrained passive motion of the shoulder complex. Biplane radiographic images of the shoulder were acquired at 60 Hz (85 kV, 200 mA, 3 ms, inter-beam angle = 60°, source-to-detector distances = 170 cm), while passively moving the humerus through two simulated motions using a pulley system: (1) scapular plane abduction (SAB) and (2) internal/external rotation (IR/ER) in 90° of arm abduction with approximate motion frequency of 0.4–1.2 HZ.

Following tantalum bead implantation in each bone of interest, CT imaging was acquired on a clinical CT scanner (Siemens Somaton Sensation 64; Forchheim, Germany; kVp = 140) with a voxel size of 0.4 × 0.4 × 0.6 $mm^3$.

### 2.3. Image analysis

Three-dimensional models of the humerus and scapula were manually segmented from reconstructed CT and MRI images (Mimics; Materialise NV; Leuven, Belgium). Coordinate systems for the CT-based bone models were defined using anatomical landmarks following ISB recommendations (Fig. 1) (Wu et al., 2005).

#### 2.3.1. 3D-3D rigid-body co-registration

To align the coordinate systems in the CT and MRI models, the MRI-based image volume was aligned to the CT-based image volume using 3D-3D rigid-body co-registration. First, surface-based registration was applied to find the initial alignment using the iterative closest point algorithm (Besl and McKay, 1992). The surface-based registration required the accurate segmentation of the image volume. However, in MRI, geometric distortion near the bone-tissue interfaces diminishes the segmentation accuracy (Sumanaweera et al., 1994). Therefore, following the surface-based registration, the voxel-based auto-registration was performed for fine alignment using a custom MATLAB script (R2016a, Mathworks Inc.; Natick, USA). A voxel-based registration approach uses most of the available information in the bone image volume, rather than only external edges and thereby reduces the dependency of the registration on the accuracy of segmentation. Because both the MR and CT images are informative of the same underlying anatomy, there will be mutual information between them (Wells et al., 1996), thereby, a normalized mutual information similarity measure was used to maximize the similarity between them (Appendix B) (Studholme, 1999). The accuracy of image registration was visually verified using various anatomic bony landmarks recognizable in the corresponding CT and MRI slices. For the scapula these landmarks included the coracoid process, acromial process, superior angle, inferior angle, supra-glenoid tubercle, and infra-glenoid tubercle. For the humerus, the landmarks included the lesser tubercle, deltoid tuberosity, intertubercular groove, and greater tuberosity. Note that because the MRI field of view only enclosed the proximal humerus, the humeral epicondyles could not be used for the comparison. 3D volume visualization was also used for visual verification because it can better reflect global geometric information (Fig. 2).

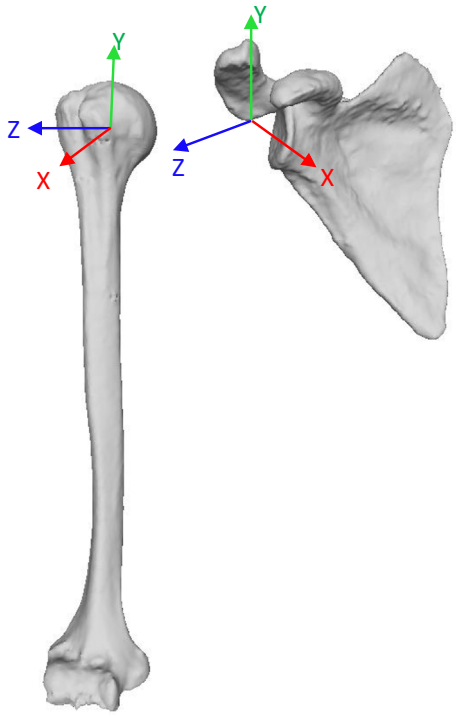


**Fig. 1.** Local coordinate systems for the humerus and the scapula. The local coordinate systems were defined using ISB anatomical reference frames (Wu et al., 2005); X: posterior/anterior; Y: inferior/superior; Z: medial/lateral.

#### 2.3.2. 2D-3D auto-registration algorithm

Our automatic 2D-3D registration algorithm, written as a MATLAB script, consists of the following steps:

(1) Digitally reconstructed radiographs (DRRs) were constructed from the 3D image volumes (CT and MRI) using a perspective ray casting approach to accurately represent

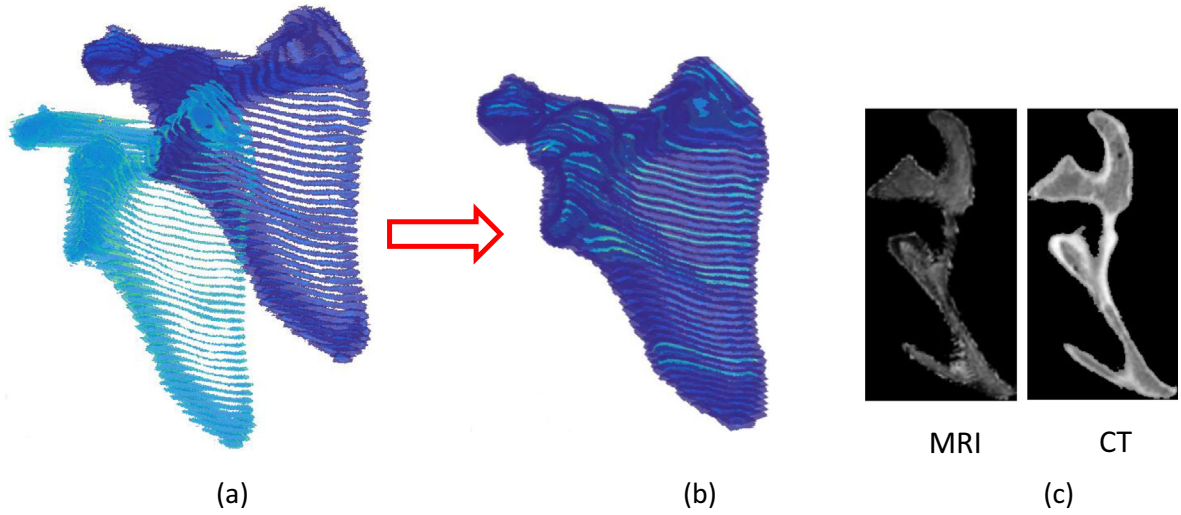


**Fig. 2.** Verifying the accuracy of 3D-3D image automatic registration of two volumetric CT and MRI image datasets using volume visualization: (a) before registration, (b) after registration and (c) using anatomic bony landmarks in the CT and MRI slices.

the cone-beam X-ray image reconstruction process (Fig. 3) (Han et al., 1999; Jacobs et al., 1998; Siddon, 1984). A view ray is traced back toward the x-ray focal point per image pixel, traversing the 3D grid volume. Voxel samples are taken along the ray and composited to a single intensity value. To accelerate the ray casting process, the image plane was restricted to the region of interest, given the bone projection area in the previously tracked frame plus a custom margin in all directions (customized by activity speed).

(2) In order to improve the algorithm's ability to find a solution, image filtering was applied to both the DRR and radiographs. The images were contrast-enhanced using a histogram-equalization algorithm. A median filter was also applied to reduce image noise. Then, a Sobel edge detector filter was applied to enhance edges by computing an approximation of the gradient of the image intensity function (Engel, 2006). See Appendix C for more details of the filter parameters.

(3) Correspondence between DRRs and radiography images is calculated using a normalized cross correlation as the similarity measure (Appendix D) (Sonka et al., 1993).

Note that for the CT-based registration, the edge information is added to both the radiographs and DRRs and a combination of edge and intensity information is used for the 2D-3D registration. However, because the MRI imaging volumes and radiography imaging modality provide different tissue contrast, only edge-information is used to measure the correlation coefficient between the MRI-based DRRs and the radiographs.

(4) A Nelder-Mead Simplex optimization algorithm is used to maximize the similarity by adjusting the six degree-of-freedom (DOF) motion parameters until the desired correlation has been reached (Lagarias et al., 1998). This optimization method is advantageous for the 2D/3D registration because it deals well with the noise in the cost function (i.e. due to image noise). In this study, each frame of data requires approximately 30–60 s of computing time for the solution of each bone to converge depending on factors such as the amount of bone motion relative to the previous frame and the size of the region under the DRR. As such, "typical" processing for a file of shoulder elevation motion at 1 Hz would be approximately 60–120 min. The computation time is recorded from un-optimized MATLAB code running on an Intel Quad Core processor, 3.50 GHz and 16 GB RAM. Computation time can be improved by applying an efficient implementation of the registration algorithm using the C/C ++ programming language.

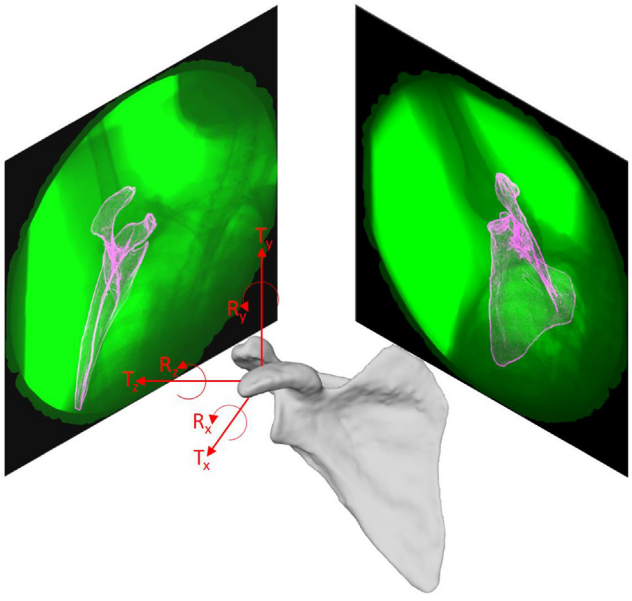


**Fig. 3.** 2D-3D auto-registration program. The pair of DRRs constructed from the 3D bone models were automatically matched to each set of two 2D calibrated and undistorted radiography images. Optimization is used to maximize the similarity by adjusting the six degree-of-freedom (DOF) motion parameters until the desired correlation has been reached. Green: Video-radiography image; pink: DRR. (For interpretation of the references to colour in this figure legend, the reader is referred to the web version of this article.)

For the first frame of the dynamic radiography data, the bone pose was defined manually. Then, these parameters were used as initial input to our auto-registration program. The pair of DRRs constructed from the 3D bone models were automatically matched to each set of two 2D calibrated and undistorted radiography images (Fig. 3). Because of the higher frame rate (60 Hz) that biplane radiographic images were acquired at compared to the

activity speeds (approximate motion frequency of 0.4–1.2 Hz), the movement of bone models between subsequent radiographic frames was minimal. Therefore, the optimization algorithm was often able to converge to the global minimum due to the accurate initial guess from the previous frame. However, in cases in which image noise affected the automatic registration and objects were not well-registered, the operator could manually intervene (e.g. by increasing the optimization iteration or modifying the initial guess) until the results were satisfactory. In order to prevent the influence of the implanted beads on image registration, traces of the beads were removed from the CT images, by replacing the beads' pixels with neighboring pixels (Patel et al., 2012).

### 2.4. RSA analysis

To perform a comparison between 2D-3D auto-registration and RSA analysis, the 3D positions of the beads were determined relative to the bone coordinate systems by digitizing them directly from the CT volumes. The positions of the beads were tracked from the biplane radiography images using XMALab software (Brown University) (Knorlein et al., 2016), and then used to calculate frame-by-frame trajectories for each bead set and thus the corresponding bone model. See Appendix E for explanations of pose estimation algorithm used in the RSA. A cubic Plexiglas phantom with two non-coplanar bead sets (bead diameter = 1 mm; positioning tolerance = ±0.02 mm) was used to validate RSA.

### 2.5. Comparison analysis

The accuracy of the 2D-3D image registration was calculated by computing the measurement bias, precision, and root-mean-squared (RMS) error of the 2D-3D image registration results compared to the RSA for each of six DOF of the humerus, scapula, and GH joint kinematics and each matching method (CT and MRI) and motion (SAB and IR/ER). The rotation and translation kinematics for the humerus and scapula were measured relative to the global coordinate system. The GH joint kinematics was measured using a XZ'Y'' Euler rotation sequence, which describes the angle of elevation, anterior/posterior plane of elevation, and axial rotation (Phadke et al., 2011).

All frames of the data were analyzed for IR/ER. However, for SAB, data were sampled for 30 frames across early, mid, and late motion (total 90 frames) due to the large number of frames (~200 frames/shoulder). Subsequently, accuracy data were calculated by pooling across specimens.

## 3. Results

For the RSA accuracy validation, the total bias and precision errors of RSA were 0.0 ± 0.2 mm and 0.1 ± 0.2°. RMS errors for the CT-based models ranged from 0.4 to 0.5 mm and 0.1–0.5° for the scapula, and 0.7–0.9 mm and 0.5–2.0° for the humerus. Detailed results for humeral and scapular kinematics including bias and precision values are shown in Table 1. These errors corresponded with RMS errors of 0.6–1.0 mm and 0.6–2.2° for glenohumeral kinematics. Detailed results for GH kinematics including bias and precision values are shown in Table 2.

RMS errors for the MR-based models ranged from 0.6 to 1.7 mm and 0.5–1.2° for the scapula, and 1.0–1.6 mm and 1.2–2.4° for the humerus. Detailed results for humeral and scapular kinematics including bias and precision values are shown in Table 1. These errors corresponded with RMS errors of 1.3–2.2 mm and 1.2–2.6° for GH kinematics. Detailed results for GH kinematics including bias and precision values are shown in Table 2. Glenohumeral kinematic profiles for the dominant degrees of freedom (i.e. elevation angle for the SAB motion, and IR/ER rotation angle for the axial rotation motion) are shown in Fig. 4.

## 4. Discussion

For individual bone tracking, the CT-based registration was able to provide sub-millimeter and sub-degree kinematic accuracy with the exception of humeral Y (axial) rotation (≤2°), which is more difficult to measure because of its relative cylindrical symmetry. The MRI-based registration bias and precision errors were less than 1.6 mm and 1.6° for individual bone tracking, again with the exception of humeral Y (axial) rotation (≤2.4°).

The results of the CT-based registration accuracy are in the range of published results of other similar 2D-3D shoulder validation studies (Bey et al., 2006; Giphart et al., 2012; Massimini et al., 2011; Zhu et al., 2012). In a validation study of four cadaveric shoulders, the average bias and precision error for GH kinematics were reported as 0.2 ± 0.5 mm, 0.3 ± 0.3 mm, and 0.3 ± 0.4 mm for anterior-posterior, superior-inferior, and medial–lateral positions, respectively, and 0.2 ± 0.2°, 1.7 ± 1.2°, and 0.1 ± 0.8° for elevation, axial rotation, and plane of elevation respectively

**Table 1**
Humerus and scapula tracking accuracy (RMS, bias ± precision) for the CT- and MRI-based model registration compared to RSA for each of six DOF.

| | Humerus | | | | Scapula | | | |
|---|---|---|---|---|---|---|---|---|
| | CT-based | | MRI-based | | CT-based | | MRI-based | |
| *SAB* | RMS | Bias ± precision | RMS | Bias ± precision | RMS | Bias ± precision | RMS | Bias ± precision |
| AP position (mm) | 0.8 | −0.2 ± 0.6 | 1.0 | 0.1 ± 0.9 | 0.4 | 0.0 ± 0.3 | 1.7 | 0.7 ± 1.0 |
| SI position (mm) | 0.8 | −0.2 ± 1.2 | 1.0 | −0.3 ± 0.9 | 0.5 | −0.3 ± 0.3 | 1.2 | −0.3 ± 0.8 |
| ML position (mm) | 0.9 | −0.1 ± 0.9 | 1.6 | −0.6 ± 1.1 | 0.5 | 0.0 ± 0.3 | 1.2 | 0.9 ± 0.7 |
| X rotation (deg.) | 0.7 | −0.1 ± 0.9 | 1.4 | −0.1 ± 1.3 | 0.5 | 0.1 ± 0.4 | 1.2 | 0.5 ± 0.8 |
| Y rotation (deg.) | 1.6 | 0.2 ± 1.4 | 2.3 | 0.4 ± 1.9 | 0.3 | −0.1 ± 0.2 | 1.1 | 0.1 ± 0.8 |
| Z rotation (deg.) | 0.9 | 0.0 ± 0.9 | 1.6 | 0.5 ± 1.3 | 0.5 | 0.1 ± 0.4 | 1.2 | −0.5 ± 0.8 |
| *Axial rotation* | | | | | | | | |
| AP position (mm) | 0.8 | −0.1 ± 0.5 | 1.5 | 0.5 ± 1.1 | 0.5 | 0.1 ± 0.1 | 1.0 | 0.3 ± 0.4 |
| SI position (mm) | 0.8 | 0.0 ± 0.5 | 1.3 | −0.1 ± 0.9 | 0.4 | −0.3 ± 0.1 | 0.6 | 0.0 ± 0.5 |
| ML position (mm) | 0.7 | −0.1 ± 0.4 | 1.3 | 0.0 ± 0.9 | 0.4 | 0.1 ± 0.1 | 1.3 | 1.0 ± 0.4 |
| X rotation (deg.) | 0.5 | 0.1 ± 0.5 | 1.2 | 0.3 ± 1.1 | 0.1 | 0.0 ± 0.1 | 0.5 | 0.1 ± 0.2 |
| Y rotation (deg.) | 2.0 | 0.6 ± 1.7 | 2.4 | 0.9 ± 2.1 | 0.3 | −0.2 ± 0.1 | 0.6 | 0.1 ± 0.2 |
| Z rotation (deg.) | 0.9 | 0.2 ± 0.7 | 1.5 | 0.1 ± 1.4 | 0.5 | 0.2 ± 0.1 | 0.7 | 0.2 ± 0.2 |

Data presented as RMS, bias ± precision for each motion tested (SAB and axial rotation). SAB: scapular plane abduction, RMS: root-mean-squared, AP: anterior-posterior, SI: superior-inferior, ML: medial-lateral, DOF = degrees of freedom. For the humerus, the X, Y, and Z rotations corresponds to elevation, internal/external rotation, and anterior/posterior plane of elevation, respectively. For the scapula, the X, Y, and Z rotations corresponds to upward rotation, internal/external rotation, and anterior/posterior tilt, respectively.

**Table 2**
Glenohumeral kinematics accuracy (RMS, bias ± precision) for the CT- and MRI-based model registration compared to RSA for each of six DOF.

| | CT-based | | MR-based | |
|---|---|---|---|---|
| *SAB* | RMS | Bias ± precision | RMS | Bias ± precision |
| AP position (mm) | 1.0 | −0.2 ± 0.7 | 1.7 | −0.5 ± 1.3 |
| SI position (mm) | 0.7 | −0.2 ± 0.5 | 1.3 | −0.1 ± 1.3 |
| ML position (mm) | 1.0 | 0.2 ± 0.8 | 2.2 | −0.5 ± 1.5 |
| Elevation (deg.) | 0.8 | −0.2 ± 0.7 | 1.6 | −0.4 ± 1.6 |
| Axial rotation (deg.) | 1.6 | 0.4 ± 1.3 | 2.3 | 0.3 ± 1.9 |
| Plane of elevation (deg.) | 1.0 | 0.0 ± 0.8 | 2.0 | 0.5 ± 1.5 |
| *Axial rotation* | | | | |
| AP position (mm) | 1.0 | −0.2 ± 0.6 | 2.1 | 0.3 ± 1.2 |
| SI position (mm) | 0.6 | 0.1 ± 0.5 | 1.4 | 0.5 ± 1.0 |
| ML position (mm) | 1.0 | 0.1 ± 0.4 | 1.9 | −0.5 ± 1.1 |
| Elevation (deg.) | 0.6 | 0.1 ± 0.5 | 1.2 | 0.2 ± 1.1 |
| Axial rotation (deg.) | 2.2 | 0.9 ± 1.7 | 2.6 | 1.0 ± 2.1 |
| Plane of elevation (deg.) | 1.0 | 0.2 ± 0.7 | 1.8 | 0.0 ± 1.4 |

Data presented as RMS, bias ± precision for each motion tested (SAB and axial rotation). SAB: scapular plane abduction, RMS: root-mean-squared, AP: anterior-posterior, SI: superior-inferior, ML: medial-lateral, DOF = degrees of freedom.

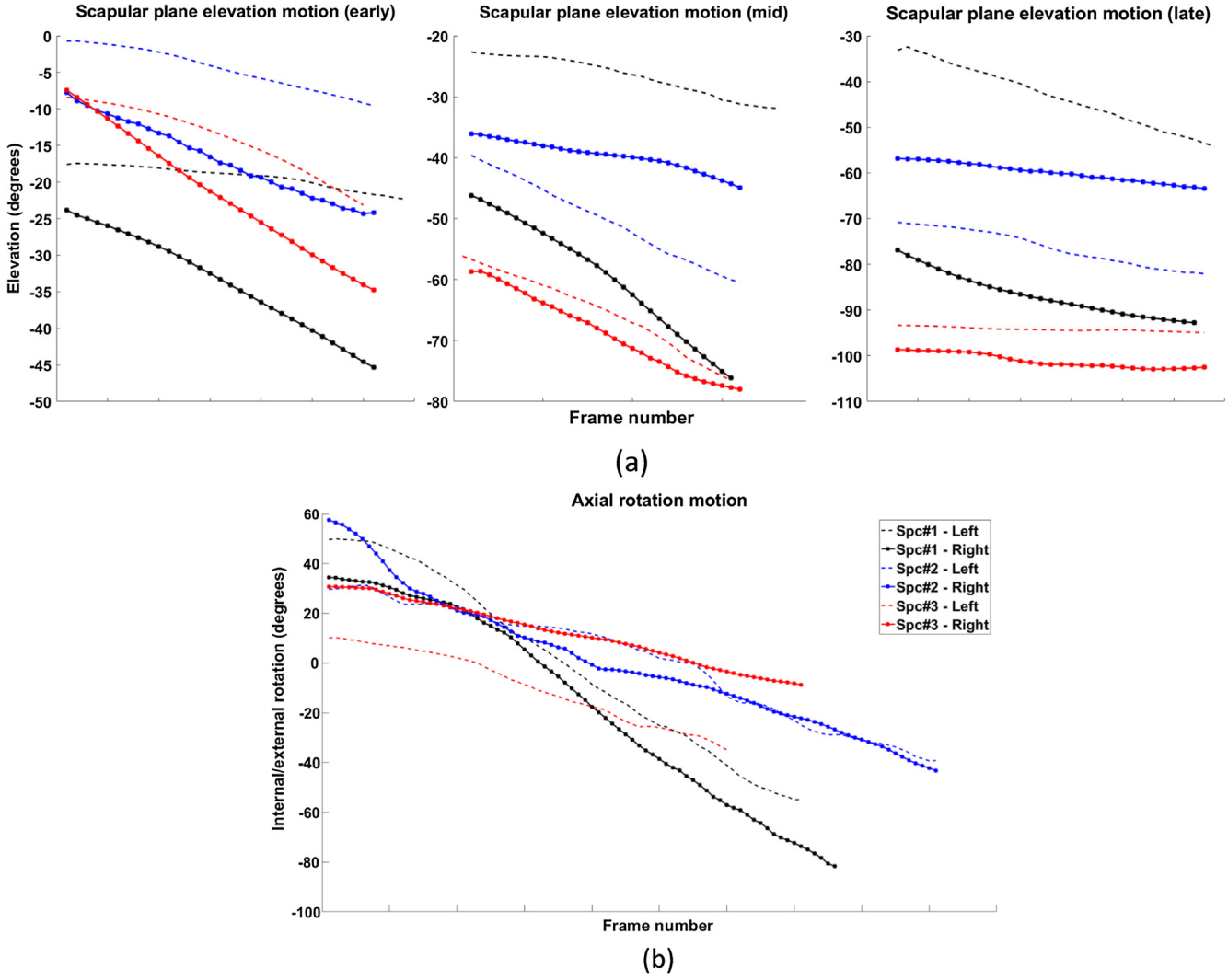


**Fig. 4.** Glenohumeral kinematics. (a) Elevation angle for scapular plane abduction (SAB) in the early, mid, and late phases of motion for each speciman (Spc). Data were sampled for 30 frames across each of the early, mid, and late phases of motion (total 90 frames) due to the large number of frames (~200 frames/shoulder); (b) Internal/external rotation (IR/ER) angle for the axial rotation motion. All frames of the data were analyzed for IR/ER.

(Giphart et al., 2012). We are unaware of any previous study of GH kinematics using MRI–based registration with which to compare our results. In a validation study of the knee joint, MRI- and CT- based models were used to validate the 3D kinematic measurement accuracy (Moro-Oka et al., 2007). For the tibiofemoral kinematics, the overall RMS errors reported were 1.0 mm for all positions and 0.5° for all rotations with the CT models and 1.3 mm and 1.4° using the MRI models. Descriptively larger errors measured in our study may in part be due to the increased challenge associated with imaging the shoulder using videoradiography compared to the knee.

Several factors likely contributed to the different shape-matching performance with the CT– and MRI–based bone models such as different image characteristics, different nominal spatial resolution, and the addition of the intensity information in the CT-based registration compared to edge information alone in MRI-based registration. In this study, the mutual information measures were also tested to maximize correspondence between DRRs generated from MRI and radiography in the 2D-3D registration algorithm. However, the optimization did not consistently converge to the correct solutions. We hypothesized that, because of information loss due to the 2D projection of 3D volume in DRR generation, DRRs generated from MRI do not share sufficient information with radiography images for the optimization to converge. But for the 3D-3D rigid body co-registration, our optimization algorithm and the normalized mutual information similarity measure could find enough information to maximize the similarity between CT and MRI image volumes.

This study was limited by validating the proposed technique on two passive shoulder activities of SAB and IR/ER rotation. However, we expect to see similar results when testing slow active multiplanar shoulder activities, because the accuracy of our automatic 2D-3D registration method mainly depends on the bone quality, activity speed, and shoulder orientation in the biplane radiography field of view. Current data are not generalizable to motion capture deviating substantially with regard to these conditions. As another limitation of this study, because a cadaveric model was used, the influence of bone motion during MRI scanning on the quality of MRI (due to the longer acquisition time of MRI) was not evaluated.

Overall, our experiment suggests that, when CT imaging is not viable or desirable, MRI-based models may also provide acceptable registration accuracy for tracking GH motion from biplane videoradiography using our automatic 2D-3D registration. In these situations, the MRI-based registration accuracy should be considered in study design, defining the clinical parameters being studied and influencing the necessary sample size, as well as qualifying the interpretation of results.

## Conflict of interest statement

The authors have no conflicts of interest related to this manuscript.

## Acknowledgment

We gratefully acknowledge the generosity of the donors and their families. Funding was provided from the Minnesota Partnership for Biotechnology and Medical Genomics (MNP IF #14.02), University of Minnesota OVPR Infrastructure Grant, Institute for Engineering in Medicine Grant, NIH/NICHD K12HD073945, NIH/NICHD F31HD087069, NIH/NIBIB P41 EB015894, and the Foundation for Physical Therapy.

## Appendix A. Supplementary material

Supplementary data to this article can be found online at https://doi.org/10.1016/j.jbiomech.2018.09.019.

## References

Akbari-Shandiz, M., Mozingo, J.D., Holmes, D.R., Zhao, K.D., 2018. An interpolation technique to enable accurate three-dimensional joint kinematic analyses using asynchronous biplane fluoroscopy. Med. Eng. Phys. 60, 109–116.
Anderst, W.J., Vaidya, R., Tashman, S., 2008. A technique to measure three-dimensional in vivo rotation of fused and adjacent lumbar vertebrae. Spine J. 8, 991–997.
Besl, P.J., McKay, N.D., 1992. Method for registration of 3-D shapes. Robot. Tentat. 14, 239–256.
Bey, M.J., Zauel, R., Brock, S.K., Tashman, S., 2006. Validation of a new model-based tracking technique for measuring three-dimensional, in vivo glenohumeral joint kinematics. J. Biomech. Eng. 128, 604–609.
Brainerd, E.L., Baier, D.B., Gatesy, S.M., Hedrick, T.L., Metzger, K.A., Gilbert, S.L., Crisco, J.J., 2010. X-ray reconstruction of moving morphology (XROMM): precision, accuracy and applications in comparative biomechanics research. J. Exp. Zool. 313, 262–279.
Engel, K., 2006. Sobel operator. In: Real-Time Volume Graphics. A K Peters, pp. 112–113.
Giphart, J.E., Elser, F., Dewing, C.B., Torry, M.R., Millett, P.J., 2012. The long head of the biceps tendon has minimal effect on in vivo glenohumeral kinematics: a biplane fluoroscopy study. Am. J. Sports Med. 40, 202–212.
Han, G., Liang, Z., You, J., 1999. A fast ray-tracing technique for TCT and ECT studies. In: Nuclear Science Symposium, 1999. Conference Record. IEEE, pp. 1515–1518.
Jacobs, F., Sundermann, E., De Sutter, B., Christiaens, M., Lemahieu, I., 1998. A fast algorithm to calculate the exact radiological path through a pixel or voxel space. J. Comput. Inf. Technol. 6, 89–94.
Knorlein, B.J., Baier, D.B., Gatesy, S.M., Laurence-Chasen, J.D., Brainerd, E.L., 2016. Validation of XMALab software for marker-based XROMM. J. Exp. Biol. 219, 3701–3711.
Lagarias, J.C., Reeds, J.A., Wright, M.H., Wright, P.E., 1998. Convergence properties of the Nelder-Mead simplex method in low dimensions. SIAM J. Optim. 9, 112–147.
Ludewig, P.M., Phadke, V., Braman, J.P., Hassett, D.R., Cieminski, C.J., LaPrade, R.F., 2009. Motion of the shoulder complex during multiplanar humeral elevation. J. Bone Joint Surg. Am. 91, 378–389.
Massimini, D.F., Warner, J.J.P., Li, G., 2011. Non-invasive determination of coupled motion of the scapula and humerus-An invitro validation. J. Biomech. 44, 408–412.
Moro-Oka, T.A., Hamai, S., Miura, H., Shimoto, T., Higaki, H., Fregly, B.J., Iwamoto, Y., Banks, S.A., 2007. Can magnetic resonance imaging-derived bone models be used for accurate motion measurement with single-plane three-dimensional shape registration? J. Orthop. Res. 25, 867–872.
Patel, P., Prajapati, A., Mishra, S., 2012. Review of different inpainting algorithms. Int. J. Comput. Appl. 59, 30–34.
Phadke, V., Braman, J.P., LaPrade, R.F., Ludewig, P.M., 2011. Comparison of glenohumeral motion using different rotation sequences. J. Biomech. 44, 700–705.
Rofsky, N.M., Lee, V.S., Laub, G., Pollack, M.A., Krinsky, G.A., Thomasson, D., Ambrosino, M.M., Weinreb, J.C., 1999. Abdominal MR imaging with a volumetric interpolated breath-hold examination. Radiology 212, 876–884.
Semelka, R.C., Armao, D.M., Elias, J., Huda, W., 2007. Imaging strategies to reduce the risk of radiation in CT studies, including selective substitution with MRI. J. Magn. Reson. Imaging 25, 900–909.
Siddon, R.L., 1984. Fast calculation of the exact radiological path for a three-dimensional CT array. Med. Phys. 12, 252–255.
Sonka, M., Hlavac, V., Boyle, R., 1993. Image Processing, Analysis, and Machine Vision. Springer.
Studholme, C., 1999. An overlap invariant entropy measure of 3D medical image alignment. Pattern Recognit. 32, 71–86.
Sumanaweera, T., Glover, G., Song, S., Adler, J., Napel, S., 1994. Quantifying MRI geometric distortion in tissue. Magn. Reson. Med. 31, 40–47.
Tashman, S., Collon, D., Anderson, K., Kolowich, P., Anderst, W., 2004. Abnormal rotational knee motion during running after anterior cruciate ligament reconstruction. Am. J. Sports Med. 32, 975–983.
Wells, W.M., Viola, P., Atsumi, H., Nakajima, S., Kikinis, R., 1996. Multi-modal volume registration by maximization of mutual information. Med. Image Anal. 1, 35–51.
Wu, G., Van Der Helm, F.C.T., Veeger, H.E.J., Makhsous, M., Van Roy, P., Anglin, C., Nagels, J., Karduna, A.R., McQuade, K., Wang, X., Werner, F.W., Buchholz, B., 2005. ISB recommendation on definitions of joint coordinate systems of various joints for the reporting of human joint motion - Part II: Shoulder, elbow, wrist and hand. J. Biomech. 38, 981–992.
Zhu, Z., Massimini, D.F., Wang, G., Warner, J.J.P., Li, G., 2012. The accuracy and repeatability of an automatic 2D–3D fluoroscopic image-model registration technique for determining shoulder joint kinematics. Med. Eng. Phys. 34, 1303–1309.